nature chemistry

ARTICLES

https://doi.org/10.1038/s41557-019-0313-y

A closed cycle for esterifying aromatic hydrocarbons with CO_2 and alcohol

Dianne J. Xiao[1], Emma D. Chant[1], Amy D. Frankhouser[1], Ying Chen[2], Allison Yau[1], Nancy M. Washton[2] and Matthew W. Kanan[1]*

The ability to functionalize hydrocarbons with CO_2 could create opportunities for high-volume CO_2 utilization. However, current methods to form carbon–carbon bonds between hydrocarbons and CO_2 require stoichiometric consumption of very resource-intensive reagents to overcome the low reactivity of these substrates. Here, we report a simple semi-continuous cycle that converts aromatic hydrocarbons, CO_2 and alcohol into aromatic esters without consumption of stoichiometric reagents. Our strategy centres on the use of solid bases composed of an alkali carbonate (M_2CO_3, where $M^+ = K^+$ or Cs^+) dispersed over a mesoporous support. Nanoscale confinement disrupts the crystallinity of M_2CO_3 and engenders strong base reactivity at intermediate temperatures. The overall cycle involves two distinct steps: (1) CO_3^{2-}-promoted C–H carboxylation, in which the hydrocarbon substrate is deprotonated by the supported M_2CO_3 and reacts with CO_2 to form a supported carboxylate (RCO_2M); and (2) methylation, in which RCO_2M reacts with methanol and CO_2 to form an isolable methyl ester with concomitant regeneration of M_2CO_3.

Methods to insert CO_2 into hydrocarbon C–H bonds could enable its use as a C_1 feedstock for commodity carboxylic acids and their derivatives (for example, esters, amides and nitriles)[1,2]. In addition to providing high-volume applications for CO_2, such processes may also offer practical advantages over current industrial routes to carboxylic acids, which require aerobic oxidations under highly corrosive and potentially hazardous conditions and utilize more complex hydrocarbon starting materials[3–5]. However, functionalizing hydrocarbons with CO_2 faces significant thermodynamic and kinetic hurdles. For example, aromatic hydrocarbon esterification with CO_2 is slightly exothermic but entropically disfavoured, which results in a positive $\Delta G°$ and low equilibrium conversion at any temperature (Fig. 1a)[6–8]. Moreover, the high homolytic and heterolytic bond strengths of hydrocarbon C–H bonds result in a large kinetic barrier for C–H activation, which must occur before C–C bond formation. Previously, researchers have converted hydrocarbons and CO_2 into carboxylates (C–H carboxylation) using highly resource-intensive stoichiometric reagents to provide a driving force and overcome the kinetic barriers[9–15]. In particular, C–H carboxylation of benzene to form benzoate has been performed using *n*-BuLi and *t*-BuOK (ref. [11]), Al^0 and $AlCl_3$ (ref. [12]) or $AlMe_{1.5}(OEt)_{1.5}$ (ref. [13]) as limiting reagents. Although benzoate produced by these methods could be protonated with acid and converted into carboxylic acid derivatives using conventional chemistry, all of these carboxylation reagents require multiple synthetic steps from primary mineral and/or hydrocarbon feedstocks, are non-regenerable and more expensive than any high-volume carboxylic acid derivative, and generate superstoichiometric waste.

We recently showed that CO_3^{2-} can serve as a base promoter for C–H carboxylations at intermediate temperatures (200–350 °C) in reaction media composed of Cs^+ or K^+ carboxylates[16–18]. The CO_3^{2-}-containing alkali carboxylates exhibit remarkable basicity in this temperature regime, allowing for carboxylation of ordinarily non-acidic C–H bonds ($pK_a > 40$ in organic solvent). This chemistry is most effective for converting a monocarboxylate to a dicarboxylate, wherein the monocarboxylate serves as both the substrate and the reaction medium. We also showed that the addition of a caesium carboxylate co-salt (for example, caesium isobutyrate) to Cs_2CO_3 enables carboxylation of benzene at elevated temperatures[16]. Although this approach avoids the use of a strong organic base or Lewis acid, the co-salt partially decomposes under the reaction conditions and greatly complicates product isolation. Moreover, the reaction showed no selectivity for mono- versus di- or tricarboxylation.

To overcome these limitations, we envisioned a cycle that uses a solid base form of M_2CO_3 to promote hydrocarbon C–H carboxylation, and then a combination of CO_2 and alcohol to convert the resulting carboxylate into an isolable ester with concomitant regeneration of M_2CO_3 (Fig. 1b). Since the net transformation is hydrocarbon esterification with CO_2 and alcohol, this two-step cycle is still subject to the low equilibrium conversion dictated by $\Delta G°$. However, the use of a solid carrier facilitates product isolation and reactant recycling. In addition, the formation of water as a byproduct makes it possible in principle to drive esterification to much higher conversion by employing a sorbent to remove water in one or both steps. Thermal regeneration of the water sorbent would serve as the energy input to compensate for $\Delta G°$.

Results and discussion

The simplicity of the hydrocarbon esterification cycle belies the challenge of rendering a gas–solid reaction between a hydrocarbon and M_2CO_3. Previous studies have shown that thermally pretreated metal oxides featuring pairs of basic and Lewis acidic surface sites (that is, O^{2-} and exposed metal cations) catalyse hydrocarbon hydrogen/deuterium exchange and olefin isomerization via heterolytic C–H activation at moderate temperatures, but this reactivity is rapidly poisoned by CO_2 or H_2O via the formation of inert surface carbonates and hydroxides[19–22]. One previous report in the patent literature has described benzene carboxylation with ball-milled

[1]Department of Chemistry, Stanford University, Stanford, CA, USA. [2]Environmental Molecular Sciences Laboratory, Pacific Northwest National Laboratory, Richland, WA, USA. *e-mail: mkanan@stanford.edu

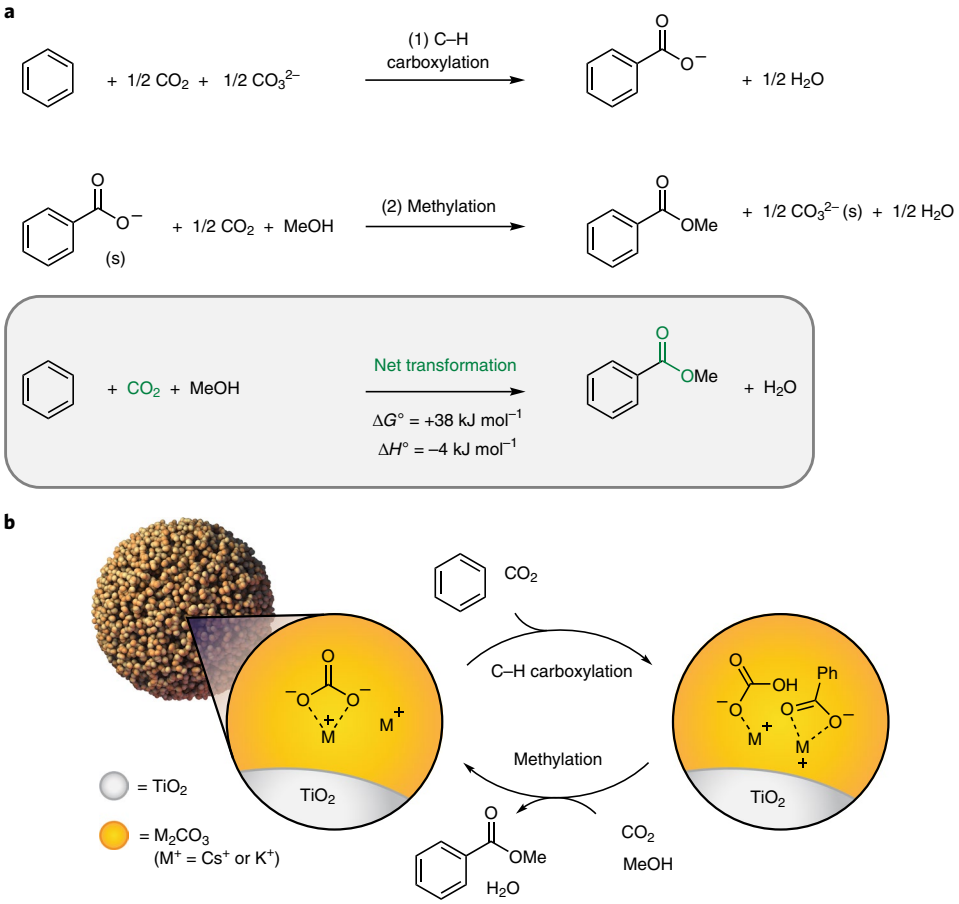

Fig. 1 | A closed cycle for the esterification of benzene using CO_2 and methanol. a, General outline of a closed, two-step cycle for aromatic hydrocarbon esterification that consumes no resource-intensive stoichiometric reagents; $\Delta G°$ and $\Delta H°$ are the standard free energy change and standard enthalpy change, respectively, for the esterification of benzene with CO_2 and MeOH with all species in the gas phase at 298 K. **b**, Hydrocarbon esterification using carbonate dispersed over mesoporous TiO_2 (M_2CO_3/TiO_2). In the first step, supported M_2CO_3 deprotonates benzene, forming a carbanion that rapidly reacts with CO_2 to generate a surface-bound benzoate. In the second step, the surface-bound benzoate reacts with MeOH and CO_2, forming a volatile methyl ester and regenerating M_2CO_3/TiO_2. Note that, for simplicity, we have shown the $MHCO_3$ species. However, under carboxylation conditions (380–440 °C), $MHCO_3$ is thermally unstable and will decompose back into M_2CO_3, releasing 0.5 equivalents of H_2O and CO_2.

K_2CO_3 and CO_2 to form potassium terephthalate at 400 °C, but the reaction required extreme pressures (350–1,750 bar) and the use of CdF_2 and aluminium carbide as stoichiometric additives[23].

We hypothesized that dispersing M_2CO_3 over a mesoporous material would engender reactivity with hydrocarbon substrates in the absence of stoichiometric additives by disrupting the bulk M_2CO_3 structure and increasing the surface area (Fig. 1b). A number of supported M_2CO_3 materials have previously been synthesized, but they were investigated as carbon capture materials[24], catalysts for transesterification[25] or precursors to supported alkali oxides[26], and never used for hydrocarbon activation.

Synthesis and characterization of M_2CO_3/TiO_2. TiO_2 was initially chosen as the M_2CO_3 support because of its excellent chemical and thermal stability. To avoid inhomogeneities in M_2CO_3 loading, we used a sol-gel method to synthesize monodisperse, mesoporous TiO_2 spheres[27]. Scanning electron microscopy (SEM) confirmed a uniform particle size of ~800 nm (Fig. 2a), and characterization of the pore sizes by the Barrett–Joyner–Halenda method indicated a narrow distribution of pore diameters with a peak at 11 nm (Supplementary Fig. 1). The porous structure is composed of anatase-phase TiO_2 nanocrystallites, and displays a Brunauer–Emmett–Teller surface area of 110 $m^2 g^{-1}$ and a pore volume of 0.32 $cm^3 g^{-1}$. K_2CO_3 or Cs_2CO_3 was dispersed over the TiO_2 via incipient wetness impregnation followed by solvent evaporation at 150 °C[28]. A single impregnation step resulted in a loading of 560 µmol M_2CO_3 per gram of TiO_2 (1×), which corresponds to 15.4 wt% Cs_2CO_3 and 7.2 wt% K_2CO_3. Higher loadings were prepared by iterative impregnation and drying steps, leading to materials with 1.12 mmol (2×) and 1.68 mmol (3×) M_2CO_3 per gram TiO_2. As expected, reductions in the surface area and pore volume were observed on increasing the M_2CO_3 loading (Supplementary Table 1).

A suite of characterization methods showed that, at low loadings (1×), the M_2CO_3 in the resulting M_2CO_3/TiO_2 material is very finely dispersed within the pores, such that most CO_3^{2-} moieties are exposed to guest molecules. Scanning transmission electron microscopy elemental mapping studies of Ti and Cs/K confirmed that the M_2CO_3 is distributed uniformly both within a single particle and between particles (Supplementary Figs. 2 and 3). SEM images of Cs_2CO_3/TiO_2 (1×) revealed no obvious morphological changes on Cs_2CO_3 loading, and no large Cs_2CO_3 particles were visible on the surface of the TiO_2 support (Fig. 2a). No new peaks were observed in the powder X-ray diffraction (pXRD) pattern of Cs_2CO_3/TiO_2 (1×) or K_2CO_3/TiO_2 (1×) relative to bare TiO_2, indicating the absence of crystalline M_2CO_3 particles within the pores (Fig. 2c and Supplementary Fig. 4). Infrared spectra were collected

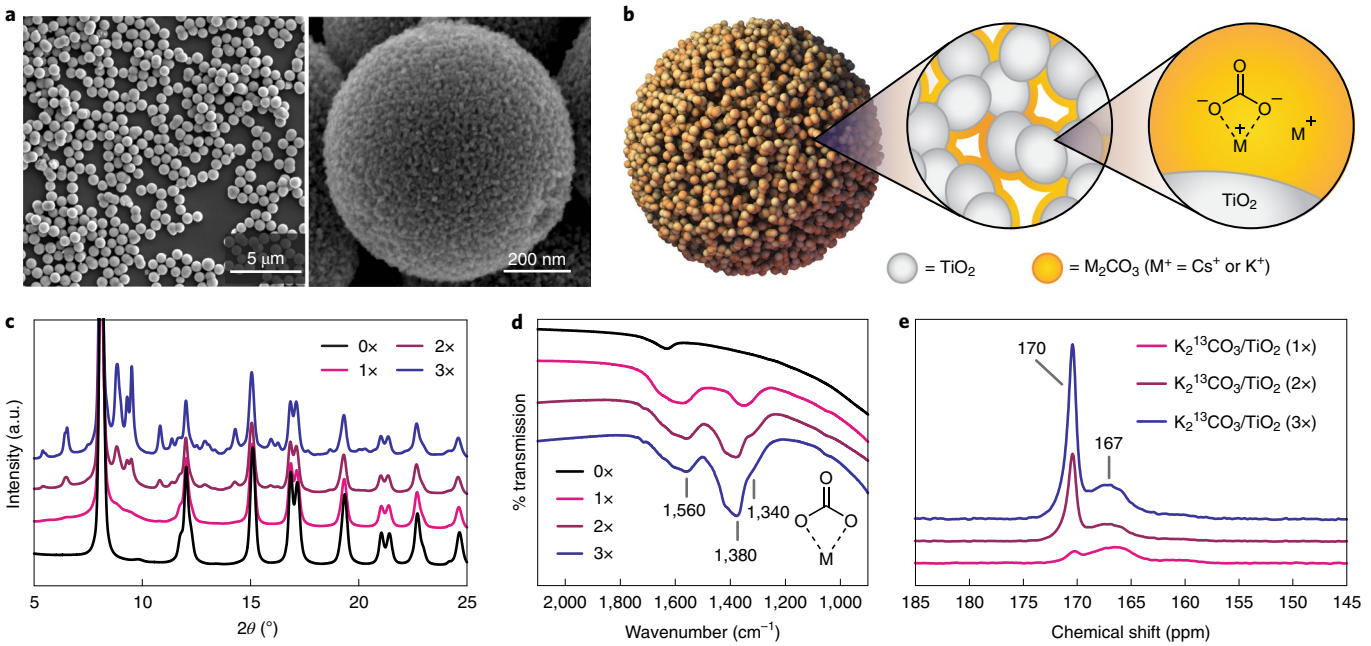

Fig. 2 | Characterization and proposed model of M_2CO_3/TiO_2. a, SEM images of monodisperse, mesoporous TiO_2 spheres (left) and Cs_2CO_3/TiO_2 (1×) (right). No obvious morphological changes were observed on Cs_2CO_3 loading, and no large Cs_2CO_3 particles were visible on the surface of the TiO_2 support. **b**, A highly simplified model of M_2CO_3/TiO_2 (1×), consistent with all obtained characterization data. At low loadings (1×), the M_2CO_3 is amorphous and very finely dispersed, such that the majority of CO_3^{2-} is surface exposed and chelated to M^+ cations ($M^+ = Cs^+$ or K^+). Larger crystalline domains of M_2CO_3 are formed only at higher loadings (2–3×). **c**, pXRD patterns ($\lambda = 0.496944$ Å) of Cs_2CO_3/TiO_2 as a function of carbonate loading. At low loadings (1×), the supported Cs_2CO_3 is essentially amorphous. Peaks associated with bulk-like, crystalline Cs_2CO_3 do not appear until much higher loadings (2–3×). **d**, Infrared spectra of Cs_2CO_3/TiO_2 as a function of carbonate loading. The pair of peaks at 1,560 and 1,340 cm^{-1} are assigned to bidentate CO_3^{2-} or similar surface-bound species featuring reduced symmetry. The single peak at 1,380 cm^{-1} that grows in at higher loadings is assigned to bulk-like, symmetrically coordinated CO_3^{2-}. **e**, Solid-state ^{13}C NMR spectra of $K_2{}^{13}CO_3/TiO_2$ as a function of carbonate loading. Two distinct CO_3^{2-} species are observed. The broad resonance at 167 ppm is assigned to disordered surface CO_3^{2-}, whereas the sharper resonance at 170 ppm is assigned to bulk-like CO_3^{2-}.

as a function of loading to probe the local CO_3^{2-} coordination environment (Fig. 2d). Bulk M_2CO_3 displays one infrared-active C–O stretching vibration at ~1,400 cm^{-1}. This vibration splits into two distinct bands as the symmetry around the anion is lowered, such as when the CO_3^{2-} is surface bound[29,30]. At low Cs_2CO_3 loadings, the C–O stretching region of the Cs_2CO_3/TiO_2 infrared spectrum is dominated by a pair of peaks at 1,340 and 1,560 cm^{-1}. The observed splitting of 220 cm^{-1} appears most consistent with CO_3^{2-} bound in a bidentate fashion to a weakly polarizing cation, such as Cs^+, although more complicated polydentate structures are also possible[31]. At higher loadings (2× and 3×), the finely dispersed Cs_2CO_3 species aggregate to form larger, crystalline nanoparticles within the pores. Carbonate aggregation was evidenced by the appearance and growth of new peaks associated with crystalline Cs_2CO_3 in both the pXRD patterns and the infrared spectra (Fig. 2c,d). Very similar pXRD and infrared results were obtained for K_2CO_3/TiO_2 samples (Supplementary Fig. 4).

The structure of the CO_3^{2-} species in M_2CO_3/TiO_2 was further investigated by solid-state magic angle spinning NMR spectroscopy of $K_2{}^{13}CO_3/TiO_2$ samples prepared with varied loadings (1–3×) of 98% ^{13}C-enriched K_2CO_3. Although bulk crystalline $K_2{}^{13}CO_3$ displays a single ^{13}C resonance at 170 ppm (Supplementary Fig. 5), $K_2{}^{13}CO_3/TiO_2$ samples show the appearance of an additional broad resonance centred at 167 ppm, which we have assigned as disordered surface-bound CO_3^{2-} (Fig. 2e). The broadening and upfield shift of this new resonance are consistent with previous NMR characterization of amorphous calcium carbonate[32]. Notably, although disordered amorphous calcium carbonate is known to spontaneously crystallize at temperatures below 300 °C[33], the resonance associated with surface-bound CO_3^{2-} in $K_2{}^{13}CO_3/TiO_2$ (2×) was observed via operando high-temperature magic angle spinning NMR[34,35] to remain at temperatures up to 320 °C (Supplementary Fig. 6), suggesting that the disordered carbonate species supported on TiO_2 is remarkably resistant to crystallization.

Measurement of the magnetic relaxation dynamics for $K_2{}^{13}CO_3/TiO_2$ (2×) revealed substantially different behaviour for the surface-bound species compared with the bulk-like carbonate. At room temperature, the longitudinal relaxation time (T_1) decreased from 221 s for the 170 ppm resonance to 23 s for the 167 ppm resonance (Supplementary Fig. 5). This result is consistent with a disordered structure for the surface-bound species in which the CO_3^{2-} has increased mobility[36]. The intensity of the 167 ppm resonance relative to the 170 ppm resonance decreases as the loading is increased (Fig. 2e). Along with the pXRD and infrared characterization results, this observation suggests that bulk-like domains of M_2CO_3 form at higher M_2CO_3/TiO_2 loadings. Quantification of ^{13}C peak areas indicated that surface-bound CO_3^{2-} accounts for ~60% of ^{13}C content in $K_2{}^{13}CO_3/TiO_2$ (1×), compared with only ~30% in $K_2{}^{13}CO_3/TiO_2$ (3×) (Supplementary Fig. 7). These values were corroborated by surface titration studies in benzene (Supplementary Fig. 8)[29,37].

Benzene carboxylation and methylation. Informed by these characterization studies, we next evaluated the first step of the hydrocarbon esterification cycle: CO_3^{2-}-promoted C–H carboxylation to form a supported alkali carboxylate salt. Benzene was chosen as an initial model aromatic substrate. Carboxylation reactions were carried out by heating M_2CO_3/TiO_2 under benzene and CO_2 (2:1 ratio; 30 bar total pressure at reaction temperature) in a stainless steel batch reactor at various temperatures between 380 and 440 °C (Fig. 3a). Industrial-grade CO_2 (99.5%) was used without further

a

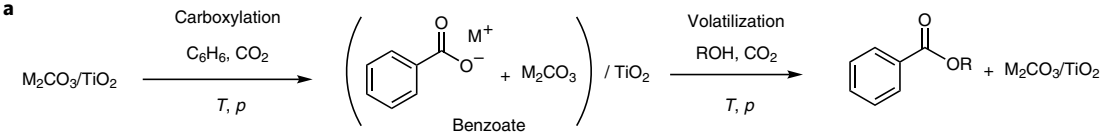

M_2CO_3 loading: 560 μmol g^{-1} TiO_2

Carboxylation

T (°C)	M^+	Time (h)	p_{CO_2} (bar)	$p_{C_6H_6}$ (bar)	Benzoate yield (μmol g^{-1} TiO_2)	Benzoate selectivity (%)
420	Cs[a]	3	20	10	–	–
420	K[a]	3	20	10	–	–
380	Cs	3	20	10	37	96
400	Cs	3	20	10	56	92
420	Cs	3	20	10	92	88
440	Cs	0.5	20	10	78	89
400	K	3	20	10	25	91
420	K	3	20	10	70	88
440	K	3	20	10	99	90

Volatilization

T (°C)	M^+	ROH	p_{CO_2} (bar)	p_{ROH} (bar)	Yield (%)
250	Cs	MeOH	1.2	1.8	70%
280	K	MeOH	1.2	1.8	80%
380	K	H_2O	1.6	1.4	30%

100% selectivity for benzoate;
all di- and tricarboxylates remain on the support

[a]Unsupported control experiment; bulk M_2CO_3 powders were used.

b

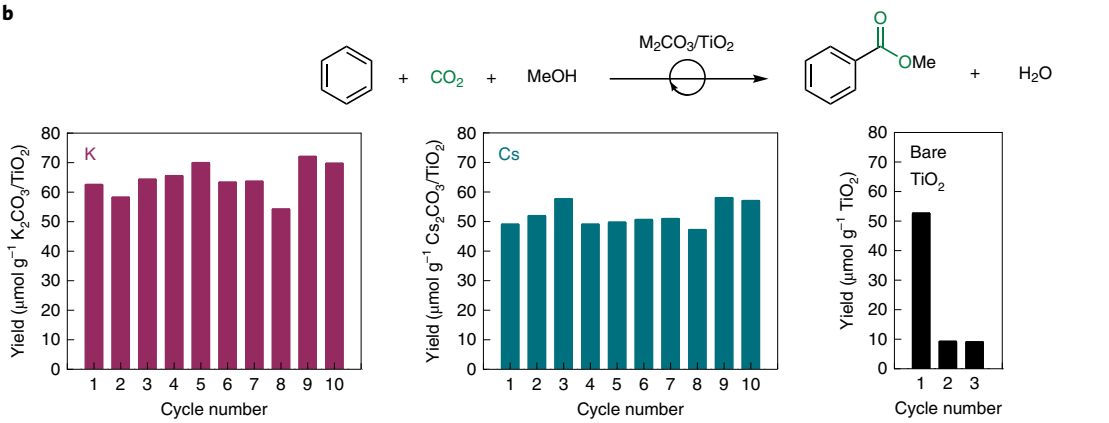

c

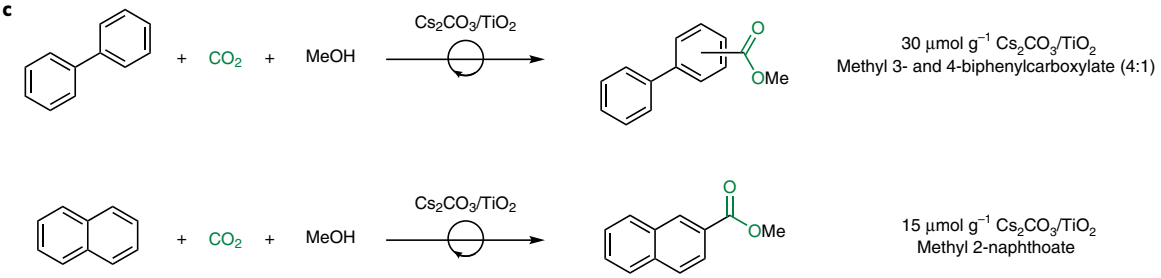

Fig. 3 | Carboxylation, volatilization and cycling results for K and Cs_2CO_3/TiO_2 (1×). a, Initial optimization of benzene carboxylation (left table) and volatilization (right table) at various temperatures (T) and pressures (p). Benzene carboxylation was observed on M_2CO_3/TiO_2 (1×) at temperatures as low as 380 °C, and was not observed at all on bulk M_2CO_3. Volatilization of the surface-bound benzoate could be accomplished using either MeOH/CO_2 to form methyl benzoate or H_2O/CO_2 to form benzoic acid. **b**, Cycling results for K_2CO_3/TiO_2 (1×), Cs_2CO_3/TiO_2 (1×) and bare TiO_2. Although the M_2CO_3/TiO_2 (1×) materials seem indefinitely stable to cycling, bare TiO_2 is deactivated after just one cycle. K_2CO_3/TiO_2 (1×) cycling conditions: benzene carboxylation was performed at 440 °C for 3 h, and methylation was performed at 280 °C for 1 h at 20 ml min^{-1}. Cs_2CO_3/TiO_2 cycling conditions: benzene carboxylation was performed at 440 °C for 0.5 h, and methylation was performed at 250 °C for 1 h at 100 ml min^{-1}. TiO_2 cycling conditions: benzene carboxylation was performed at 420 °C for 3 h, and methylation was performed at 280 °C for 1 h. **c**, Cs_2CO_3/TiO_2 (1×) also facilitates the esterification of other simple aromatic hydrocarbons in addition to benzene, such as biphenyl and naphthalene (the yields shown are the average of five cycles).

purification. The products were quantified by ^{1}H NMR with an internal standard (Supplementary Figs. 11 and 12). We found that Cs_2CO_3/TiO_2 (1×) reacted with benzene to form caesium benzoate at temperatures as low as 380 °C, with yields reaching a maximum of 92 μmol g^{-1} TiO_2 after 3 h at 420 °C. Yields plateau above 420 °C, perhaps because benzoate decarboxylation becomes a competing decomposition pathway above this temperature[38,39]. Shorter reaction times (0.5 h) could be achieved by increasing the temperature to 440 °C. Small amounts of dicarboxylated isomers were produced along with benzoate. K_2CO_3/TiO_2 (1×) required slightly higher tem-

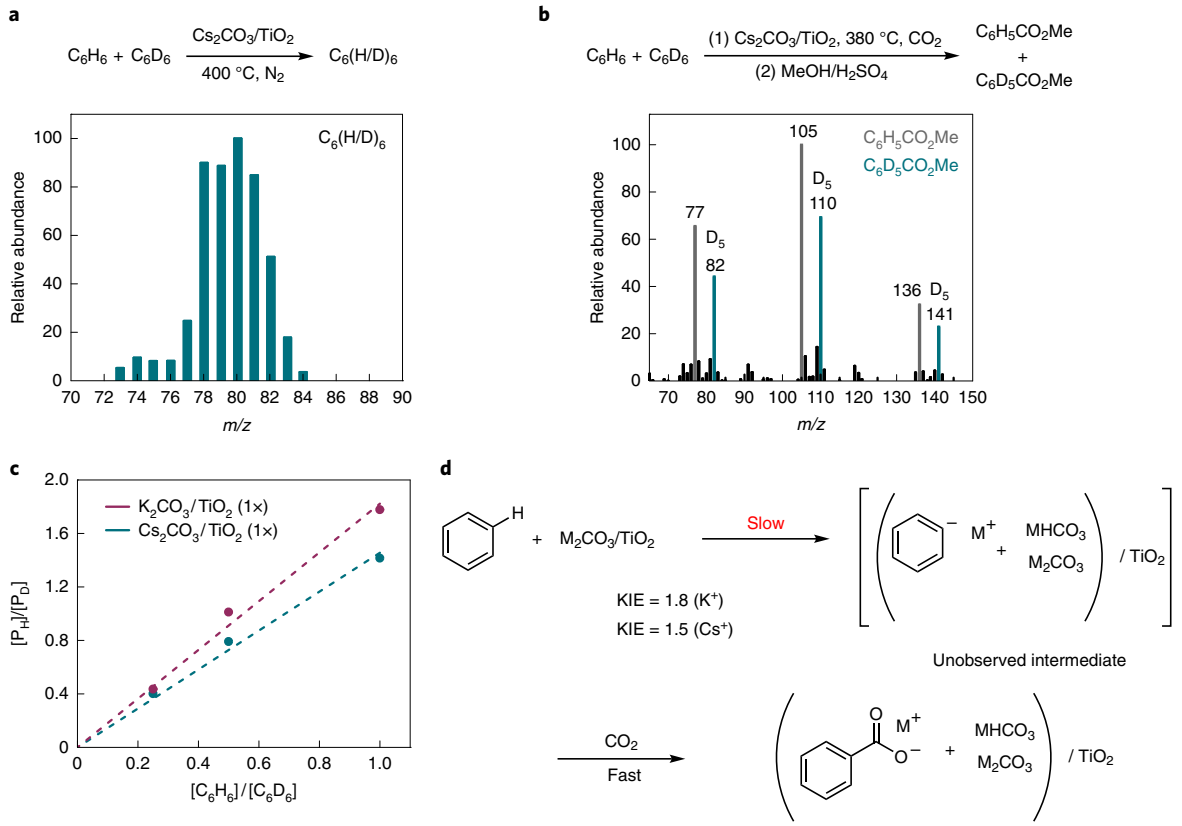

Fig. 4 | Mechanistic studies. a, In the absence of CO_2, M_2CO_3/TiO_2 catalyses benzene hydrogen/deuterium (H/D) exchange, suggesting that the carbonate surface reversibly deprotonates benzene at elevated temperatures. In the presence of Cs_2CO_3/TiO_2 (1×), a 1:1 mixture of C_6H_6 and C_6D_6 is completely scrambled after 12 h at 400 °C. **b**, KIE values for benzene C–H carboxylation were measured via intermolecular competition experiments. A primary KIE was observed, consistent with slow C–H deprotonation relative to CO_2 addition. The mass spectrum shows the relative amounts of methyl benzoate-H_5 and D_5 obtained from carboxylation of a 1:1 mixture of C_6H_6 and C_6D_6 using Cs_2CO_3/TiO_2 (1×) at 380 °C for 0.5 h. **c**, Ratio of protiated to deuterated products obtained from carbonate-promoted carboxylation of 1:1, 1:2 and 1:4 mixtures of C_6H_6 and C_6D_6 (380 °C; 0.5 h). KIE values of 1.8 and 1.5 were obtained for K_2CO_3 and Cs_2CO_3/TiO_2 (1×), respectively. **d**, Proposed mechanism featuring irreversible benzene deprotonation, consistent with the hydrogen/deuterium exchange and KIE experiments. Note that, for simplicity, we have shown the $MHCO_3$ species. However, under carboxylation conditions (380–440 °C), $MHCO_3$ is thermally unstable and will decompose back into M_2CO_3, releasing 0.5 equivalents of H_2O and CO_2.

peratures to produce comparable yields, forming 99 μmol g^{-1} TiO_2 after 3 h at 440 °C. Commercial mesoporous TiO_2 featuring broad particle and pore size distributions could also be used as M_2CO_3 supports instead of monodisperse spheres, although the lower surface area and pore volume of these materials led to lower yields (Supplementary Table 6).

In sharp contrast with the M_2CO_3/TiO_2 materials, no carboxylation products were observed when subjecting Cs_2CO_3 or K_2CO_3 powders to the same reaction conditions (Fig. 3a). Consistent with this result, benzoate yields did not increase for M_2CO_3/TiO_2 materials as the M_2CO_3 loading was increased beyond 1× (Supplementary Table 7). Higher M_2CO_3 loadings resulted in larger M_2CO_3 particles with bulk-like domains. These results show that disrupting the bulk structure of M_2CO_3 through confinement within mesopores is essential to engender CO_3^{2-} reactivity with benzene at low pressures.

Interestingly, mesoporous TiO_2 freshly calcined at 450 °C also promoted benzene carboxylation, yielding 84 μmol benzoate g^{-1} at 420 °C. However, we found this reactivity to be highly sensitive to H_2O vapour. On the addition of 20 μl H_2O to the reaction vessel (p_{H_2O}: ~2 bar at reaction temperature), benzoate yields plummeted to <5 μmol g^{-1}. Unlike the bare metal oxide, substantial activity was maintained by M_2CO_3/TiO_2, even in the presence of H_2O. Under similarly wet conditions, 44 μmol benzoate g^{-1} TiO_2 was formed on K_2CO_3/TiO_2 (1×) at 420 °C, compared with the 70 μmol g^{-1} TiO_2 obtained under dry conditions. Benzene activation on bare TiO_2 may rely on Lewis acidic, coordinatively unsaturated Ti^{4+} defect sites that are easily quenched by water, similar to what is observed on other activated metal oxides such as γ-Al_2O_3[19,21].

Next, we examined methods to convert the surface-bound alkali benzoates into volatile methyl esters and regenerate the CO_3^{2-} surface. Gratifyingly, benzoate methylation proceeded readily on exposure of the carboxylated M_2CO_3/TiO_2 (1×) material to a flow of MeOH-saturated CO_2. For K_2CO_3/TiO_2, after 1 h of flowing CO_2/MeOH (20 ml min^{-1}) at 3 bar and 280 °C, 80% of the benzoate was collected as methyl benzoate in a downstream cold trap; 70% methyl benzoate was collected from Cs_2CO_3/TiO_2 after 1 h at 250 °C (100 ml min^{-1}) (Fig. 3a). Gas chromatography-mass spectrometry (GC–MS) analysis of the material in the cold trap revealed trace dimethyl carbonate (DMC)—a well-known methylating agent[40]. This result suggests that methyl carbonate species (DMC or methyl carbonate ($CH_3OCO_2^-$)) formed in situ from MeOH and CO_2 are responsible for methylating benzoate (Supplementary Fig. 16). Fortuitously, methylation also served as a means of product purification, as no dicarboxylic acid esters were recovered in the cold trap. Notably, volatilization of benzoic acid was also achieved using H_2O-saturated CO_2 streams, but this process was less efficient; in an unoptimized procedure, ~30% benzoate was recovered as benzoic acid after 1 h of flowing CO_2/H_2O at 3 bar and 380 °C (Fig. 3a).

Cycling experiments and substrate scope. Having identified conditions for carboxylation and methylation, we assessed the ability of M_2CO_3/TiO_2 to catalyse a closed hydrocarbon esterification cycle over multiple iterations. When a single sample of K_2CO_3/TiO_2 (1×) was used for ten CO_2 insertion cycles, methyl benzoate was isolated as the only detectable product from each cycle with an average yield of 69 μmol methyl benzoate g^{-1} TiO_2 per cycle (which corresponds to 64 μmol g^{-1} K_2CO_3/TiO_2 per cycle) (Fig. 3b). No deactivation was observed over the ten cycles. SEM and gas sorption measurements after the ten cycles indicated slight sintering of the K_2CO_3/TiO_2 material, which evidently did not affect reactivity (Supplementary Figs. 18–20). Similar results were obtained using Cs_2CO_3/TiO_2 (1×), which produced an average yield of 52 μmol methyl benzoate g^{-1} Cs_2CO_3/TiO_2 per cycle over ten cycles. When mesoporous TiO_2 was subjected to the same cycling conditions, the yield of methyl benzoate decreased from 53 to <10 μmol g^{-1} after just one cycle (Fig. 3b). The drop in yield is a consequence of deactivation of the TiO_2 surface by MeOH during the methylation step. The resistance of M_2CO_3/TiO_2 to alcohol/H_2O deactivation is essential for sustaining robust esterification activity over multiple cycles.

Hydrocarbon esterification was readily applied to other aromatic substrates. Biphenyl esterification generated 30 μmol g^{-1} Cs_2CO_3/TiO_2 of methyl 3- and 4-biphenylcarboxylate in a 4:1 ratio (average of five cycles), and naphthalene esterification produced 15 μmol g^{-1} Cs_2CO_3/TiO_2 of methyl 2-naphthoate per cycle (average of five cycles), with methyl 1-naphthoate observed in trace quantities (Fig. 3c). Similar to benzene, methylation also served as a product purification step, as the initial carboxylation reactions for both substrates produced a complex mixture of mono and dicarboxylated isomers (Supplementary Tables 9 and 10). Together, these examples represent the synthesis of a carboxylic acid derivative using hydrocarbon and CO_2 without consuming any stoichiometric reagents. Remarkably, this challenging transformation can be performed in a closed cycle using a very simple material that is robust, easy to prepare and handle, and contains no precious metals.

Mechanistic studies. We hypothesized that the carboxylation mechanism proceeds via hydrocarbon deprotonation by M_2CO_3/TiO_2, followed by rapid reaction with CO_2 to form a surface-bound carboxylate. To test this hypothesis, we first assessed the ability of M_2CO_3/TiO_2 to deprotonate benzene through isotope exchange experiments. Under an inert atmosphere (N_2) and in the presence of Cs_2CO_3/TiO_2 (1×), a 1:1 mixture of C_6H_6:C_6D_6 (0.5 bar) showed complete hydrogen/deuterium scrambling after 12 h at 400 °C (Fig. 4a). The use of K_2CO_3/TiO_2 (1×) led to partial hydrogen/deuterium scrambling under the same conditions. No scrambling was observed in the absence of M_2CO_3/TiO_2, or when bulk M_2CO_3 powders were used (Supplementary Fig. 21). These results provide independent evidence that the M_2CO_3/TiO_2 materials are capable of heterolytic activation of aryl C–H bonds.

Competition experiments were performed to determine whether there is a kinetic isotope effect (KIE) for C–H carboxylation. Analysis of carboxylation reactions performed at 380 °C for 0.5 h in the presence of various ratios of C_6H_6 and C_6D_6 revealed KIE values of 1.8 and 1.5 for K_2CO_3 and Cs_2CO_3/TiO_2, respectively, indicating that C–H deprotonation is slow relative to CO_2 addition (Fig. 4b–d and Supplementary Fig. 22). Similar KIE values (1.8–2.3) have been observed in this temperature regime for solid base-catalysed reactions featuring rate-determining deprotonation[29]. Interestingly, hydrogen/deuterium scrambling of the benzoate product was observed when the carboxylation was performed at temperatures higher than 380 °C, or for durations longer than 0.5 h, but the C_6H_6/C_6D_6 reactants remained unscrambled. These results suggest that the mixture of benzoate and carbonate formed on benzene carboxylation is dynamic, with mobile benzoate anions undergoing reversible protonation/deprotonation and carboxylation/decarboxylation (reversible phthalate formation) over the course of the reaction.

Support effects. In addition to TiO_2, ZrO_2 (100 m^2 g^{-1}), γ-Al_2O_3 (250 m^2 g^{-1}) and ordered mesoporous carbon (CMK-3; 1,060 m^2 g^{-1})[41] were also investigated to elucidate specific support effects (Supplementary Table 11). Due to the surface hydrophobicity of mesoporous carbon, methanolic Cs_2CO_3 stock solutions were required to facilitate uniform pore impregnation. Interestingly, the C–H carboxylation step appeared relatively insensitive to chemical differences between the three oxide supports (TiO_2, ZrO_2 and γ-Al_2O_3). Specifically, the percentage of CO_3^{2-} converted into mono- and dicarboxylates was very similar for all oxide supports, and averaged between 10 and 13% (Supplementary Table 12). However, because higher mesoporous pore volumes enabled higher CO_3^{2-} loadings, Cs_2CO_3/γ-Al_2O_3 produced significantly higher absolute carboxylate yields. For example, values up to 164 μmol carboxylates g^{-1} Cs_2CO_3/γ-Al_2O_3 were observed—nearly double the amount obtained for Cs_2CO_3/TiO_2 (Supplementary Table 12). Compared with the oxide supports, ordered mesoporous carbon led to a dramatic improvement in the overall CO_3^{2-} conversion and absolute carboxylate yields. Carbonate conversions of up to 26% and absolute carboxylate yields of 359 μmol carboxylates g^{-1} Cs_2CO_3/carbon were observed when CMK-3 was used as the support (Supplementary Table 12). In contrast with the robustness of the carboxylation step, the methylation procedure is highly sensitive to the chemical identity of the support. Of the four supports investigated, M_2CO_3/TiO_2 appeared uniquely able to support both efficient formation of methyl carbonate species and carboxylate methylation. For example, no DMC was observed by GC–MS when Cs_2CO_3 supported on γ-Al_2O_3 or carbon was used, and these materials gave correspondingly low methyl ester yields (<10%) (Supplementary Fig. 16 and Supplementary Table 13). Methyl benzoate yields could be increased to 75–90% by introducing DMC vapour into the system (Supplementary Table 13). In light of these findings, future research will focus on developing novel composite materials that possess both the high mesoporous pore volumes needed for high carbonate loadings and the specific active sites required for in situ DMC formation, as well as investigating alternative processes where DMC is produced in a separate step[1,42].

Conclusion

High-volume aromatic esters are currently synthesized from hydrocarbon feedstocks in a two-step sequence of aerobic oxidation of a methyl group followed by acid-catalysed esterification. Although these transformations are substantially exergonic because of the driving force of oxidation, the challenges of controlling selectivity and handling corrosive oxidations provide incentives for alternative processes. Further advancing a carboxylation/methylation cycle towards application will require providing a controlled energy input such as water removal, to minimize reactant volumes, and further tuning of solid base materials, to accelerate the individual steps.

Methods

Synthesis of M_2CO_3/TiO_2. Monodisperse TiO_2 spheres were synthesized according to a previously reported procedure[27] and calcined in air (450 °C; 2 h). Calcined TiO_2 (1.00 g) was added to a 20-ml glass vial and impregnated with an aqueous solution of M_2CO_3 (1.75 M; 0.320 ml). To achieve homogeneous loading, the carbonate solution was added dropwise in three portions and thoroughly mixed using a spatula after each addition[28]. The glass vial was then sealed with a septum cap and placed under partial vacuum. After 12 h, the material was dried under flowing N_2 (80 °C for 0.5 h; 150 °C for 1 h) to produce M_2CO_3/TiO_2 (1×). Higher loadings (2–3×) were prepared through iterative impregnation and drying steps.

Carboxylation of aromatic substrates. *Benzene carboxylation procedure.* Small stainless steel batch reactors (total volume: ~27.5 ml) were built from single-ended miniature sample cylinders (25 ml), fittings and valves purchased from Swagelok (Supplementary Fig. 9). Before each reaction, the reactor was dried at 120 °C in an oven for at least 3 h, then cooled to room temperature under vacuum. M_2CO_3/TiO_2 (333–600 mg) and an amount of benzene (0.90–1.00 ml) was added such that the final benzene pressure at reaction temperature (380–440 °C) was 20 bar. After benzene addition, the reactor was sealed, attached to a stainless steel gas dosing

manifold, and degassed by freeze-pump thawing. CO_2 (50 psig, or 4.5 bar) was dosed into the reactor at room temperature (10 bar at reaction temperature). The reactor was then removed from the manifold, wrapped in heat tape and insulation, and heated to the desired temperature at a rate of 20 °C min^{-1}. After the reaction, the reactor was cooled to room temperature, depressurized and dismantled. For direct analysis of carboxylation products, the soluble salts were separated from the support via aqueous extraction (3 × 10 ml; 70 °C), followed by filtration through a syringe filter (0.2 µm pores; polyvinylidene fluoride (PVDF)). The aqueous extract was dried and the alkali salt products were analysed by ^{1}H NMR in D_2O. For cycling studies, the reactor was depressurized and dismantled, excess benzene was evaporated (150 °C under N_2), and the solid contents of the reactor were directly transferred into the U-shaped reactor used for the volatilization studies.

Biphenyl carboxylation procedure. M_2CO_3/TiO_2 (333–600 mg) and biphenyl (600 mg, or 7.5 bar at 420 °C) were loaded into a dried stainless steel reactor. The reaction setup and workup were identical to benzene, except that the excess biphenyl was removed by washing with Et_2O before either product extraction or cycling studies.

Naphthalene carboxylation procedure. M_2CO_3/TiO_2 (500 mg) and naphthalene (250 mg, or 3.8 bar at 400 °C) were loaded into a dried stainless steel reactor. The reaction setup and workup were identical to benzene, except that the excess naphthalene was removed by sublimation before either product extraction or cycling studies.

Volatilization of aromatic carboxylates. Volatilization experiments were conducted in a U-shaped stainless steel reactor equipped with an inline filter (0.5 µm) in the vertical portion to hold the sample (typically 333–600 mg) in place (Supplementary Fig. 9). The partial pressure of ROH (methanol or H_2O) in the gas phase was controlled by heating an upstream bubbler. Volatile products were collected in a downstream cold trap (−78 °C) or base trap. Before flowing CO_2 (100 ml min^{-1}), the system was first pressurized with CO_2 and the reactor and bubbler were pre-heated to the desired temperatures.

Volatilization studies on K_2CO_3/TiO_2 (1×). For methylation of benzene carboxylation products, the reactor was set to 280 °C, the methanol bubbler was heated to 80 °C and the total pressure was set to 3 bar. The CO_2 flow rate was set to 20 ml min^{-1} and the reaction duration was 1 h. For protonation of benzoate using H_2O/CO_2, the reactor was set to 380 °C, the H_2O bubbler was set to 110 °C and the total pressure was set to 3 bar. The CO_2 flow rate was set to 100 ml min^{-1}, and the reaction duration was 3 h.

Volatilization studies on Cs_2CO_3/TiO_2 (1×). For methylation of benzene carboxylation products, the reactor was set to 250 °C, the methanol bubbler was heated to 80 °C and the total pressure was set to 3 bar. The CO_2 flow rate was set to 100 ml min^{-1} and the reaction duration was 1 h. Similar conditions were used for the methylation of biphenyl and naphthalene carboxylation products, except the reactor temperature was 280 °C and the total reaction duration was 2 h.

Volatilization product analysis. For volatilizations using methanol, the cold trap was dismantled from the apparatus and the methanol solution was gently sonicated to remove dissolved CO_2. Methyl ester products were analysed directly by high-performance liquid chromatography.

Data availability

The main data supporting the findings of this study are included in the paper and its Supplementary Information files. Additional raw data (NMR spectra, mass spectra and so on) are available from the corresponding author on reasonable request.

Received: 29 April 2019; Accepted: 17 July 2019;
Published online: 26 August 2019

References

1. Artz, J. et al. Sustainable conversion of carbon dioxide: an integrated review of catalysis and life cycle assessment. *Chem. Rev.* **118**, 434–504 (2018).
2. Liu, Q., Wu, L., Jackstell, R. & Beller, M. Using carbon dioxide as a building block in organic synthesis. *Nat. Commun.* **6**, 5933 (2015).
3. Röhrscheid, F. Carboxylic acids, aromatic. *Ullmann's Encyclopedia of Industrial Chemistry* (Wiley-VCH, 2000).
4. Ohara, T. et al. Acrylic acid and derivatives. *Ullmann's Encyclopedia of Industrial Chemistry* (Wiley-VCH, 2011).
5. Kubitschke, J., Lange, H. & Strutz, H. Carboxylic acids, aliphatic. *Ullmann's Encyclopedia of Industrial Chemistry* (Wiley-VCH, 2014).
6. *CRC Handbook of Chemistry and Physics* (CRC, 2017).
7. Guthrie, J. P., Pike, D. C. & Lee, Y.-C. Equilibrium constants and heats of formation of methyl esters and *N*,*N*-dimethyl amides of substituted benzoic acids. *Can. J. Chem.* **70**, 1671–1683 (1992).
8. Steele, W. V., Chirico, R. D., Cowell, A. B., Knipmeyer, S. E. & Nguyen, A. Thermodynamic properties and ideal-gas enthalpies of formation for methyl benzoate, ethyl benzoate, (*R*)-(+)-limonene, *tert*-amyl methyl ether, *trans*-crotonaldehyde, and diethylene glycol. *J. Chem. Eng. Data* **47**, 667–688 (2002).
9. Cai, X. & Xie, B. Direct carboxylative reactions for the transformation of carbon dioxide into carboxylic acids and derivatives. *Synthesis* **45**, 3305–3324 (2013).
10. Wang, X., Wang, H. & Sun, Y. Synthesis of acrylic acid derivatives from CO_2 and ethylene. *Chem* **3**, 211–228 (2017).
11. Schlosser, M., Jung, H. C. & Takagishi, S. Selective mono- or dimetalation of arenes by means of superbasic reagents. *Tetrahedron* **46**, 5633–5648 (1990).
12. Olah, G. A. et al. Efficient chemoselective carboxylation of aromatics to arylcarboxylic acids with a superelectrophilically activated carbon dioxide–Al_2Cl_6/Al system. *J. Am. Chem. Soc.* **124**, 11379–11391 (2002).
13. Suga, T., Mizuno, H., Takaya, J. & Iwasawa, N. Direct carboxylation of simple arenes with CO_2 through a rhodium-catalyzed C–H bond activation. *Chem Commun* **50**, 14360–14363 (2014).
14. Wu, J.-F. et al. Mechanistic insight into the formation of acetic acid from the direct conversion of methane and carbon dioxide on zinc-modified H–ZSM-5 zeolite. *J. Am. Chem. Soc.* **135**, 13567–13573 (2013).
15. Patil, U. et al. Low temperature activation of methane over a zinc-exchanged heteropolyacid as an entry to its selective oxidation to methanol and acetic acid. *Chem. Commun.* **50**, 12348–12351 (2014).
16. Banerjee, A., Dick, G. R., Yoshino, T. & Kanan, M. W. Carbon dioxide utilization via carbonate-promoted C–H carboxylation. *Nature* **531**, 215–219 (2016).
17. Dick, G. R., Frankhouser, A. D., Banerjee, A. & Kanan, M. W. A scalable carboxylation route to furan-2,5-dicarboxylic acid. *Green Chem.* **19**, 2966–2972 (2017).
18. Banerjee, A. & Kanan, M. W. Carbonate-promoted hydrogenation of carbon dioxide to multicarbon carboxylates. *ACS Cent. Sci.* **4**, 606–613 (2018).
19. Sattler, A. Hydrogen/deuterium (H/D) exchange catalysis in alkanes. *ACS Catal.* **8**, 2296–2312 (2018).
20. Utiyama, M. Exchange reaction of methane with deuterium over solid base catalysts. *J. Catal.* **53**, 237–242 (1978).
21. Joubert, J. et al. Heterolytic splitting of H_2 and CH_4 on γ-alumina as a structural probe for defect sites. *J. Phys. Chem. B* **110**, 23944–23950 (2006).
22. Hattori, H. Heterogeneous basic catalysis. *Chem. Rev.* **95**, 537–558 (1995).
23. Bruno, B., Hubert, S. & Werner, S. Process for the introduction of carboxyl groups into aromatic hydrocarbons. US patent US2948750A (1960).
24. Lee, S. C. et al. CO_2 absorption and regeneration of alkali metal-based solid sorbents. *Catal. Today* **111**, 385–390 (2006).
25. Lukić, I., Krstić, J., Jovanović, D. & Skala, D. Alumina/silica supported K_2CO_3 as a catalyst for biodiesel synthesis from sunflower oil. *Bioresour. Technol.* **100**, 4690–4696 (2009).
26. Yamaguchi, T., Zhu, J.-H., Wang, Y., Komatsu, M. & Ookawa, M. Supported K-salts as a new solid base catalyst. *Chem. Lett.* **26**, 989–990 (1997).
27. Chen, D. et al. Synthesis of monodisperse mesoporous titania beads with controllable diameter, high surface areas, and variable pore diameters (14–23 nm). *J. Am. Chem. Soc.* **132**, 4438–4444 (2010).
28. Deng, X., Chen, K. & Tüysüz, H. Protocol for the nanocasting method: preparation of ordered mesoporous metal oxides. *Chem. Mater.* **29**, 40–52 (2017).
29. Ono, Y. & Hattori, H. in *Solid Base Catalysis* 11–68 (Springer, 2011).
30. Busca, G. & Lorenzelli, V. Infrared spectroscopic identification of species arising from reactive adsorption of carbon oxides on metal oxide surfaces. *Mater. Chem.* **7**, 89–126 (1982).
31. Kantschewa, M., Albano, E. V., Ertl, G. & Knözinger, H. Infrared and X-ray photoelectron spectroscopy study of K_2CO_3/γ-Al_2O_3. *Appl. Catal.* **8**, 71–84 (1983).
32. Nebel, H., Neumann, M., Mayer, C. & Epple, M. On the structure of amorphous calcium carbonate—a detailed study by solid-state NMR spectroscopy. *Inorg. Chem.* **47**, 7874–7879 (2008).
33. Albéric, M. et al. The crystallization of amorphous calcium carbonate is kinetically governed by ion impurities and water. *Adv. Sci.* **5**, 1701000 (2018).
34. Walter, E. D. et al. *Operando* MAS NMR reaction studies at high temperatures and pressures. *J. Phys. Chem. C* **122**, 8209–8215 (2018).
35. Mehta, H. S. et al. A novel high-temperature MAS probe with optimized temperature gradient across sample rotor for in-situ monitoring of high-temperature high-pressure chemical reactions. *Solid State Nucl. Magn. Reson.* **102**, 31–35 (2019).
36. Bloembergen, N., Purcell, E. M. & Pound, R. V. Relaxation effects in nuclear magnetic resonance absorption. *Phys. Rev.* **73**, 679–712 (1948).
37. Tanabe, K. & Yamaguchi, T. Basicity and acidity of solid surfaces. *J. Res. Inst. Catal. Hokkaido Univ.* **11**, 179–184 (1964).
38. Van Deun, R. et al. Alkali-metal salts of aromatic carboxylic acids: liquid crystals without flexible chains. *Eur. J. Inorg. Chem.* **2005**, 563–571 (2005).

39. Dabestani, R., Britt, P. F. & Buchanan, A. C. Pyrolysis of aromatic carboxylic acid salts: does decarboxylation play a role in cross-linking reactions? *Energy Fuels* **19**, 365–373 (2005).
40. Shieh, W.-C., Dell, S. & Repič, O. Nucleophilic catalysis with 1,8-diazabicyclo[5.4.0]undec-7-ene (DBU) for the esterification of carboxylic acids with dimethyl carbonate. *J. Org. Chem.* **67**, 2188–2191 (2002).
41. Jun, S. et al. Synthesis of new, nanoporous carbon with hexagonally ordered mesostructure. *J. Am. Chem. Soc.* **122**, 10712–10713 (2000).
42. Santos, B. A. V., Silva, V. M. T. M., Loureiro, J. M. & Rodrigues, A. E. Review for the direct synthesis of dimethyl carbonate. *ChemBioEng Rev.* **1**, 214–229 (2014).

Acknowledgements

We thank the Global Climate and Energy Project, TomKat Center for Sustainable Energy and Camille and Henry Dreyfus Foundation for support of this work. D.J.X. acknowledges the Arnold and Mabel Beckman Foundation for a postdoctoral fellowship. A.D.F. acknowledges support from a NASA Space Technology Research Fellowship. We thank L. Darago for assistance with collecting powder diffraction data, and the Karunadasa laboratory for use of their Micromeritics ASAP 2020. Part of this work was performed at the Stanford Nano Shared Facilities, supported by the National Science Foundation under award ECCS-1542152. GC–MS data were collected at the Vincent Coates Foundation Mass Spectrometry Laboratory at Stanford University Mass Spectrometry. Powder diffraction data were collected at Beamline 12.2.2 at the Advanced Light Source, and Beamline 11-BM at the Advanced Photon Source. The Advanced Light Source is supported by the Director, Office of Science, Office of Basic Energy Sciences of the US DOE under contract number DE-AC02-05CH11231. Use of the Advanced Photon Source at Argonne National Laboratory was supported by the US Department of Energy, Office of Science, Office of Basic Energy Sciences under contract number DE-AC02-06CH11357. Solid-state NMR was performed using EMSL (grid.436923.9)—a DOE Office of Science User Facility sponsored by the Office of Biological and Environmental Research.

Author contributions

D.J.X. and M.W.K. conceived and designed the experiments. D.J.X. and E.D.C. performed all of the experiments except the solid-state NMR and transmission electron microscopy studies. A.D.F. and Y.C. performed the solid-state NMR studies. A.Y. performed the transmission electron microscopy studies. N.M.W., Y.C. and A.D.F. conceived and designed the solid-state NMR experiments. D.J.X. and M.W.K. wrote the initial draft of the paper, and all authors contributed to the final version.

Competing interests

The authors declare no competing interests.

Additional information

Supplementary information is available for this paper at https://doi.org/10.1038/s41557-019-0313-y.

Reprints and permissions information is available at www.nature.com/reprints.

Correspondence and requests for materials should be addressed to M.W.K.

Publisher's note: Springer Nature remains neutral with regard to jurisdictional claims in published maps and institutional affiliations.